

Ductile and brittle yielding in thermal and athermal amorphous materials

Hugh J. Barlow, James O. Cochran and Suzanne M. Fielding¹

¹*Department of Physics, Durham University, Science Laboratories, South Road, Durham DH1 3LE, UK*

We study theoretically the yielding of sheared amorphous materials as a function of increasing levels of initial sample annealing prior to shear, in three widely used constitutive models and three widely studied annealing protocols. In thermal systems we find a gradual progression, with increasing annealing, from smoothly “ductile” yielding, in which the sample remains homogeneous, to abruptly “brittle” yielding, in which it becomes strongly shear banded. This progression arises from an increase with annealing in the size of an overshoot in the underlying stress-strain curve for homogeneous shear, which causes a shear banding instability that becomes more severe with increasing annealing. “Ductile” and “brittle” yielding thereby emerge as two limiting cases of a continuum of yielding transitions, from gradual to catastrophic. In contrast, athermal systems with a stress overshoot always show brittle yielding at low shear rates, however small the overshoot.

Amorphous materials include soft glasses such as dense colloids, emulsions, foams and microgels [1–5], as well as hard molecular and metallic glasses [6, 7]. Under low loads or small deformations, such materials show solid-like behaviour. Under higher loads or larger deformations, they yield plastically. For some systems, the dynamical process whereby an initially solid-like sample yields to give a finally fluidised flow is rather smooth and gradual [8–16]. Others instead yield abruptly, with catastrophic sample failure [17]. For both “ductile” materials, which yield smoothly and gradually, and “brittle” materials, which yield abruptly and catastrophically, understanding the statistical physics of yielding is the focus of intense current interest. Theories have been put forward based on a first order transition in a replica theory [18, 19]; a critical point in an elastoplastic model [20, 21]; a directed percolation transition [22, 23]; and a spinodal [24–28]. Microscopic precursors to yielding have recently been observed in soft materials [29–31].

Recent mean field calculations [32, 33] have suggested that the underlying stress-strain relation, $\Sigma(\gamma)$, for an athermal amorphous material undergoing quasistatic shear displays a qualitative change in form from the lower to the upper curve in Fig. 1a) as the degree to which a sample is annealed prior to shear increases. Poorly annealed samples (lower curve) then yield in a smoothly “ductile” way. Well annealed samples (upper curve) instead show catastrophic “brittle” yielding, as the stress drops precipitously once the overhang is reached. In this scenario, “ductile” and “brittle” yielding are separated by a random critical point, at which the stress-strain curve switches between two qualitatively different shapes with increasing annealing. Particle simulations were argued to agree with this scenario [32].

Here we propose an alternative scenario, in which the underlying stress-strain curve for homogeneous shear has an overshoot, rather than an overhang, followed by a regime of negative slope, $\partial_\gamma \Sigma < 0$. In thermal systems, where $k_B T$ is important (*e.g.* compared to local energy barriers for particle rearrangements), a state of initially homogeneous shear becomes linearly unstable to the formation of shear bands in this negatively sloping

regime [34–36], with the severity of banding (defined below) after an (adimensionalised) stress drop of magnitude $\Delta\Sigma$ from the stress maximum scaling as $\exp(\Delta\Sigma)$ in the limit of slow shear. A large stress drop (strong annealing) thus causes severe banding and correspondingly brittle failure, whereas a small stress drop (weak annealing) causes only weak banding, and failure remains ductile: Fig. 1b). In slowly sheared athermal systems, in contrast, the severity of banding diverges (at the level of a linear instability calculation) as the overshoot is approached as $1/\partial_\gamma \Sigma$. Slowly sheared athermal systems accordingly show brittle failure for any size of stress drop, however small: Fig. 1c). We substantiate these scenarios both analytically and numerically in a thermal fluidity model [37] and an athermal elastoplastic model [38]; and numerically [39] in the soft glassy rheology model [40] in both thermal and athermal regimes. Crucially, in neither thermal nor athermal scenario does a critical point of the kind in Fig. 1a) separate ductile and brittle yielding.

For consistency with the vocabulary adopted in Ref. [32], we use the term “brittle” to characterise abrupt yielding in which the rate of failure is much larger than the rate of the imposed deformation, and in which the strain becomes strongly localised within the sample, but with a caveat that we quote from [32]: “Although this phenomenon is not accompanied by the formation of regions of vacuum, as it happens in the fracture of brittle

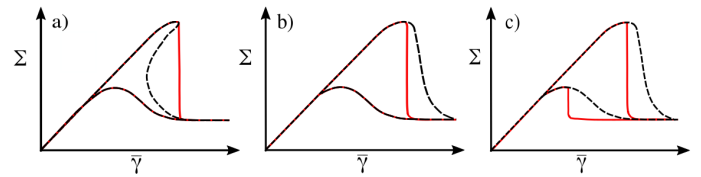


FIG. 1. Schematic shear stress *vs.* strain in different possible scenarios for ductile and brittle yielding: as suggested (a) in Ref. [32, 33], and here for (b) thermal and (c) athermal systems. In each case the upper(lower) curve is for a better(less well) annealed sample. Dashed lines: theoretical curve with homogeneous shear artificially enforced. Solid lines: precipitous drop from (a) stress overhang, or (b,c) from homogeneous curve due to shear banding, giving “brittle” yielding.

materials, the macroscopic avalanche taking place at the discontinuous yielding transition does resemble a crack induced by a brittle fracture". Indeed, our calculations and those of Ref. [32] are performed at fixed volume, disallowing the opening of an air gap. We suggest, however, that the formation of a severe high shear band in abrupt yielding will, in studies at fixed pressure, indeed lead to the rapid opening of an air gap.

We consider a sample prepared by some time $t = 0$ with some level of annealing (defined below) then sheared for all $t > 0$ between infinite flat parallel plates at $y = 0, L_y$ by moving the top plate at speed $\dot{\gamma}L_y$ in the positive \hat{x} direction. The shear is assumed incompressible and inertialess. As is standard practice, we restrict all velocities $v(y, t)$ to the main flow direction \hat{x} , and gradients to \hat{y} . The local shear rate $\dot{\gamma}(y, t) = \partial_y v(y, t)$, may vary across y due to shear banding. The spatially average imposed shear rate $\bar{\dot{\gamma}} = \int_0^{L_y} dy \dot{\gamma}(y, t) / L_y$. We track only the shear component of the stress, $\Sigma_{xy}(t) = \sigma_{xy}(y, t) + \eta \dot{\gamma}(y, t)$, with an elastoplastic contribution $\sigma_{xy}(y, t)$ and a Newtonian solvent contribution of viscosity η . Force balance requires $\partial_y \Sigma_{xy} = 0$. Hereafter we drop the xy subscript for clarity. For the dynamics of the elastoplastic stress σ , we consider three different constitutive models: a thermal continuum fluidity model [37], an athermal elastoplastic model [38] and the soft glassy rheology model [40], separately in thermal and athermal regimes [39].

Thermal systems – As a simple model of thermal systems we consider a continuum fluidity model [37], which supposes a Maxwell-type constitutive equation:

$$\partial_t \sigma(y, t) = G\dot{\gamma} - \sigma/\tau. \quad (1)$$

Here G is a constant modulus and τ is a stress relaxation time, which has its own dynamics:

$$\partial_t \tau(y, t) = 1 - \frac{|\dot{\gamma}|\tau}{1 + |\dot{\gamma}|\tau_0} + \frac{l_o^2}{\tau_0} \partial_y^2 \tau. \quad (2)$$

The first term on the RHS captures ageing, in which the timescale for stress relaxation increases linearly with the time t_w for which a sample is aged before any deformation commences. The second term captures rejuvenation by deformation, with τ_0 a microscopic timescale that sets the limiting value for τ as $\dot{\gamma} \rightarrow \infty$. The mesoscopic length l_o describes the tendency for the relaxation time of a mesoscopic region to equalise with its neighbours.

We consider a sample aged (annealed) for a time t_w before shear commences at time $t = 0$, such that $\tau(y, t = 0) = t_w$. To seed heterogeneity, we add noise in each numerical timestep Dt as $\sigma(y, t + Dt) = \sigma(y, t) + r\delta\sqrt{Dt} \cos(\pi y/L_y)$, with r chosen from a top hat distribution between -0.5 and $+0.5$, and δ small. In both this model and the athermal one below, we rescale stress, time and length so that $G = \tau_0 = L_y = 1$. The solvent viscosity $\eta \ll G\tau_0 = 1$ is unimportant to the physics we describe. We use typical values $\eta = 0.01 - 0.05$, but find no changes to our results on reducing η further.

Fig. 2a) shows as dashed lines the stress $\Sigma(\bar{\gamma})$ as a function of the accumulating strain $\bar{\gamma} = \dot{\gamma}t$, calculated

by imposing that the shear must remain homogeneous across the sample, for several values of the sample age t_w at a single value of the imposed shear rate $\dot{\gamma}$. Each curve shows an initially solid-like elastic regime in which the stress increases linearly with strain. At late times (large strains), the sample flows plastically with a constant value of the shear stress. For intermediate times (and strains), the stress shows an overshoot that increases in amplitude with increasing degree of sample annealing prior to shear (increasing t_w): an older sample shows a larger initial regime of elastic response before yielding into a finally flowing state.

We then performed separate calculations in which shear bands are allowed to form. The resulting stress-strain curves are shown by solid lines in Fig. 2a). For poorly annealed samples, each curve still follows that of the corresponding homogeneous calculation, to good approximation, indicating that the shear field remains homogeneous (or nearly so), with yielding occurring in a smoothly gradual (“ductile”) way. For well annealed samples, in contrast, the stress-strain curve of the heterogeneous calculation only follows that of the homogeneous one until just after the stress overshoot. It then drops precipitously as the sample becomes strongly shear banded, causing abrupt (“brittle”) yielding.

For each individual deformation experiment, defined by the values of $(\dot{\gamma}, t_w)$, we denote by S_{\max} the absolute value of the maximally negative value of $\partial_{\dot{\gamma}} \Sigma$ (with the maximisation performed over all times during the deformation). This quantifies the abruptness of the stress drop during yielding. We further denote by B_{\max} the degree of shear banding, again maximised over all times during the deformation. (At any time t , or strain $\bar{\gamma}(t)$, we define the degree of shear banding $B(\bar{\gamma})$ as the maximum minus minimum local strain rate across the sample, normalised by $\bar{\dot{\gamma}}$.) This quantifies the severity of shear banding during yielding. These quantities are plotted as a function of sample age in Fig. 2b), again for a fixed $\dot{\gamma}$. A regime of gradual yielding (low S_{\max}) and near homogeneous deformation (low B_{\max}) for poorly annealed samples (low t_w) crosses over into a regime of precipitous yielding (high S_{\max}) and strong banding (high B_{\max}) at high t_w . This crossover is explored in the full plane of $\dot{\gamma}, t_w$ in Fig. 3. For $\dot{\gamma} \ll 1$ it occurs at $\dot{\gamma} \approx 10^m/t_w$, with $m \approx 4.5$. Deviations from this scaling at higher $\dot{\gamma}$ should be disregarded, because the model is itself only valid for $\dot{\gamma} \ll 1$. Increasing strain localisation [36] and decreasing notch fracture toughness [41, 42] with decreasing initial ‘effective temperature’ have been seen in the STZ model.

To understand these results, we perform a linear stability analysis for how strongly shear bands will form during any deformation experiment, by writing the system’s state as the sum of a time-dependent homogeneous base state (as would pertain in a theoretically idealised deformation in which shear banding is prohibited), plus an initially small heterogeneous precursor to any shear bands: $\dot{\gamma}(y, t) = \bar{\dot{\gamma}} + \delta\dot{\gamma}(t) \exp(iky)$, $\sigma(y, t) = \bar{\sigma}(t) + \delta\sigma(t) \exp(iky)$, $\tau(y, t) = \bar{\tau}(t) + \delta\tau(t) \exp(iky)$. Sub-

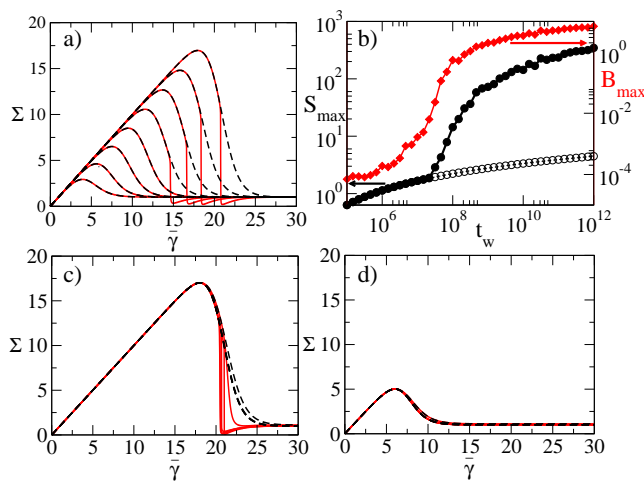


FIG. 2. **a)** Stress *vs.* strain in thermal fluidity model with homogeneous flow enforced (dashed lines) and shear banding allowed (solid lines). Imposed shear rate $\bar{\gamma} = 10^{-3}$, waiting times $t_w = 10^5, 10^6 \dots 10^{12}$ in curves left to right. **b)** Left vertical axis: steepest negative slope in stress-strain curve with homogeneous flow enforced (open circles) and allowing banding (closed black circles) *vs.* sample age t_w , for fixed $\bar{\gamma} = 10^{-3}$. Right vertical axis: corresponding maximum degree of shear banding. (S_{\max} and B_{\max} each averaged over 10 – 60 runs at each t_w .) **c)** and **d)** show curves in the same format as **a)**, but now for a fixed large stress peak $\Sigma_{\max} = 17.0$ **(c)** or small stress peak $\Sigma_{\max} = 5.0$ **(d)**, for imposed $\bar{\gamma} = 10^{-5}, 10^{-4} \dots 10^{-1}$. Steeper stress drop for smaller $\bar{\gamma}$ in **c)**. $\eta = 0.05, \delta = 0.01\bar{\gamma}, l_0 = 10^{-3}, Dt = 0.01, Dy = 1/3000$.

stituting these into the model equations and expanding to first order in the amplitude of the heterogeneity, we find [39] the degree of shear banding $\delta\dot{\gamma}(t)/\bar{\gamma}$ after a stress drop of magnitude $\Delta\Sigma$ from the stress overshoot to scale as $(\delta\dot{\gamma}_0/\bar{\gamma})\exp(\Delta\Sigma)$ in the limit $\bar{\gamma} \rightarrow 0$, with $\delta\dot{\gamma}_0/\bar{\gamma}$ the small initial heterogeneity due to noise. Systems with a small stress overshoot therefore remain almost homogeneous and show “ductile” yielding, whereas those with a large stress overshoot will show strong shear banding and “brittle” failure. “Ductile” and “brittle” yielding thus emerge as limiting cases, arising from a smooth variation in the height of the stress overshoot, which scales as a function of $\bar{\gamma}t_w$ for low $\bar{\gamma}$ (contour lines in Fig. 3). Deformation experiments with a high $\bar{\gamma}t_w$ thus show brittle failure at low $\bar{\gamma}$ (red region in Fig. 3 and low $\bar{\gamma}$ curves in Fig. 2c); those with low $\bar{\gamma}t_w$ show ductile yielding for all $\bar{\gamma}$ (dark blue region in Fig. 3; and Fig. 2d).

In Fig. 1 of Ref. [39], we explore “ductile” and “brittle” yielding in the soft glassy rheology model in its thermal regime. Each subpanel a)-d) of that figure is strikingly analogous to its counterpart in Fig. 1, demonstrating the same scenario as in this thermal fluidity model.

Athermal systems – As a simple model of an athermal amorphous material we consider an ensemble of elastoplastic elements, each corresponding to a local mesoscopic region of material [38]. Given a shear rate $\dot{\gamma}$, each

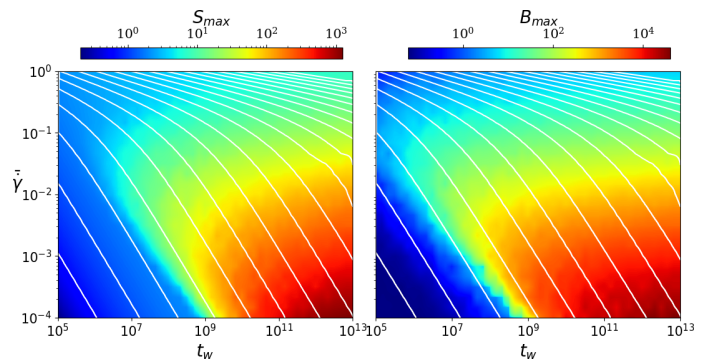


FIG. 3. Colourscale showing in thermal fluidity model **left)** steepest negative slope of stress versus strain, S_{\max} , and **right)** maximum degree of shear banding, B_{\max} , during deformation. Each coordinate pair in the plane represents an average over 10 – 60 deformation simulations, each with an initial sample age t_w and imposed shear rate $\bar{\gamma}$. Contour lines show size of stress overshoot (peak minus steady state stress) 2, 4, 6, \dots 40 (bottom left to top right). $\eta = 0.05, \delta = 0.01\bar{\gamma}, l_0 = 10^{-3}, Dt = 0.01, Dy = 1/3000$.

element builds up a local elastic shear strain l according to $\dot{l} = \dot{\gamma}$, giving a local shear stress Gl and energy $\frac{1}{2}Gl^2$, where G is a constant modulus. This stress is intermittently released by local plastic yielding events, which occur stochastically with rate $r(l) = \tau_0^{-1}$ when a local energy barrier E is exceeded, $\frac{1}{2}Gl^2 > E$, and $r(l) = 0$ otherwise, with $E = 1$ (in our units) for all elements. Here τ_0 is a microscopic attempt time. Upon yielding, any element resets its local stress to zero. The probability distribution $P(l, t)$ of local strains obeys:

$$\dot{P}(l, t) + \dot{\gamma} \partial_l P = -r(l)P + Y(t)\delta(l). \quad (3)$$

Here $Y(t) = \int dl r(l) P(l, t)$ is the ensemble average local yielding rate and $\delta(l)$ is the Dirac delta function. The total elastoplastic stress $\sigma(t) = G \int dl l P(l, t)$.

So far, we have assumed homogeneous flow in this elastoplastic model, without accounting for spatial stress propagation following any local yielding event. To account for non-uniform shear deformations, we now take $n = 1 \dots N$ streamlines at discretised flow-gradient positions $y = 0 \dots L_y$, with periodic boundary conditions. The distribution $P(l, y, t)$ on any streamline then obeys:

$$\dot{P}(l, y, t) + \dot{\gamma}(y, t) \partial_l P = -r(l)P + Y(y, t)\delta(l), \quad (4)$$

with streamline yielding rate $Y(y, t) = \int dl r(l) P(l, y, t)$ and elastoplastic stress $\sigma(y, t) = G \int dl l P(l, y, t)$. Given an imposed average shear rate $\bar{\gamma}$ across the sample as a whole, the shear rate on each streamline is calculated by enforcing force balance: $\sigma(y, t) + \eta\dot{\gamma}(y, t) = \bar{\sigma}(t) + \eta\bar{\gamma}$, with $\bar{\sigma}(t) = \frac{1}{L_y} \int dy \sigma(y, t)$. This ensures 1D stress propagation on a timescale η/G following any local yielding event, recovering the 1D projection of the Eshelby propagator of 2D lattice elastoplastic models [38].

We simulate this model by evolving $M = 80000$ elastoplastic elements on each of $N = 20$ streamlines, with

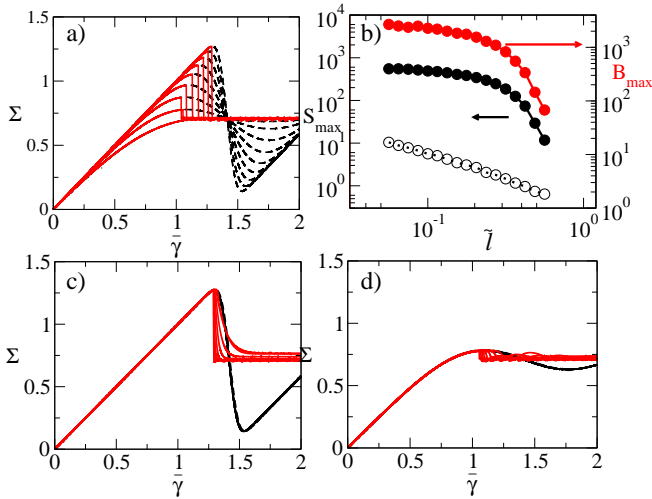


FIG. 4. **a)** Stress *vs.* strain in athermal elastoplastic model with homogeneous flow enforced (dashed lines) and shear banding allowed (solid lines). Shear rate $\bar{\gamma} = 10^{-4}$. Annealing increases with decreasing $\bar{l} = 0.562, 0.421, 0.316, 0.237, 0.177, 0.133, 0.1, 0.0749, 0.0562$ in curves left to right. **b)** Left vertical axis: steepest negative slope in stress-strain curve with homogeneous flow enforced (open symbols) and allowing banding (closed black symbols) *vs.* \bar{l} , for fixed $\bar{\gamma} = 10^{-4}$. Right vertical axis: corresponding maximum degree of shear banding. **c)** and **d)** curves in same format as **a)**, but now for fixed strong annealing $\bar{l} = 0.0562$ (**c**) or weak annealing $\bar{l} = 0.421$ (**d**), for imposed $\bar{\gamma} = 10^{-n}$ with $n = 2.00, 2.25 \dots 4.00$; steeper stress drop for smaller $\bar{\gamma}$. $\eta = 0.05, w = 0.05, N = 20, M = 80000, Dt = 0.05$.

force balance across streamlines as described. Adjacent streamlines are further weakly coupled by adjusting the stress of three randomly chosen elements on each adjacent streamline an amount $wl(-1, +2, -1)$ following any yielding event of size l , with w a small parameter, mimicking the stress diffusion term in Eqn. 2 above.

Before shear commences at time $t = 0$ we assign each element an initial local strain from a Gaussian, $P_0(l) = \exp(-l^2/2\bar{l}^2)/\sqrt{2\pi\bar{l}}$. Smaller values of \bar{l} correspond to better annealed samples. Accordingly, we characterise the degree of annealing by $1/\bar{l}$, which forms the counterpart to t_w for thermal systems above.

Fig. 4a) shows as dashed lines the stress $\Sigma(\bar{\gamma})$ as a function of accumulating strain $\bar{\gamma} = \bar{\gamma}t$, calculated by imposing that the shear must remain homogeneous, for several levels of annealing prior to shear, $1/\bar{l}$, at a single imposed $\bar{\gamma}$. Each curve shows an initially solid-like elastic regime in which the stress increases linearly with strain, before the stress declines as plastic yielding sets in. (The stress later shows a persistent oscillation known to arise in homogeneous deformation of simplified elastoplastic models [38].) As in thermal systems, more strongly annealed samples show a larger initial elastic regime.

We then performed separate calculations in which shear bands can form. The resulting stress-strain curves

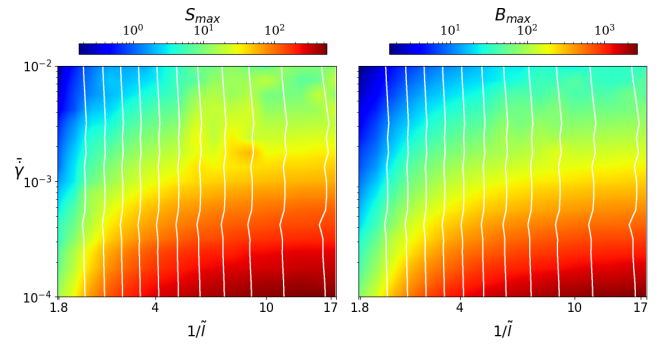


FIG. 5. Colourscale showing in athermal elastoplastic model **left)** steepest negative slope of stress versus strain, S_{\max} , and **right)** maximum degree of shear banding, B_{\max} , during deformation. Each coordinate pair represents a deformation simulation with annealing parameter $1/\bar{l}$ and imposed shear rate $\bar{\gamma}$. Contour lines show size of stress overshoot (peak minus steady state stress) 0.05, 0.10 \dots 0.55 from left to right. $\eta = 0.05, w = 0.05, N = 20, M = 80000, Dt = 0.05$.

are shown by solid lines in Fig. 4a). As the stress overshoot is reached, the stress in these heterogeneous calculations falls precipitously below that of the homogeneous calculations as shear bands form, leading to “brittle” failure. By comparing each of Figs. 4a,c,d) with its counterpart subpanel in Fig. 2, we see an important difference between thermal and athermal systems. For thermal systems, a large enough stress overshoot is required to see “brittle” failure. In contrast, athermal systems show “brittle” failure however small the overshoot. The trend to increasingly sharp failure with decreasing shear rate has been demonstrated in particle simulations of a stable glass with a large stress overshoot [43].

To explore this further, we show in Fig. 5 colourmaps of the maximum steepness of stress drop, S_{\max} , and severity of shear banding, B_{\max} , as a function of the degree of sample annealing $1/\bar{l}$ and imposed shear rate $\bar{\gamma}$. (We define the degree of banding at any time as the variance in shear rate across the sample, then maximise this quantity over the deformation simulation.) Increasing overshoot heights are shown by contour lines left to right. Even for the smallest accessible overshoot height, B_{\max} and S_{\max} increase without bound as $\bar{\gamma} \rightarrow 0$ in this athermal system, leading to “brittle” yielding.

To understand these results for athermal systems, we perform in Ref. [39] a linear stability analysis for how strongly shear bands will form during any deformation experiment. In slow shear, $\bar{\gamma} \rightarrow 0$, we find the degree of shear strain banding $\delta\gamma(t)$ to diverge as $\delta\gamma(0)/\partial_{\bar{\gamma}}\Sigma$ on approach to the stress overshoot, $\partial_{\bar{\gamma}}\Sigma = 0$. Athermal systems thus show “brittle” failure however small the stress overshoot, as indeed seen numerically in Figs. 4 and 5.

In Figs. 2 and 3 of [39], we explore yielding in the soft glassy rheology model in two different athermal protocols, demonstrating the same scenario as in Fig. 4 above for this simpler elastoplastic model. In particular, in athermal systems we always find “brittle” yielding as

$\bar{\gamma} \rightarrow 0$, however small the stress overshoot.

In this work, we have studied shear-induced yielding of amorphous materials as a function of initial sample annealing prior to shear. In thermal systems we have demonstrated a gradual progression, with increasing levels of annealing, from smoothly “ductile” yielding, in which the sample remains homogeneous, to abruptly “brittle” yielding, in which it becomes strongly shear banded. We have shown that this progression arises from an increase with annealing in the size of an overshoot in the underlying stress-strain curve for homogeneous shear. This in turn causes a shear banding instability that becomes more severe with increasing annealing. “Ductile” and “brittle” yielding thereby emerge as two limiting cases of a continuum of yielding transitions, from gradual to catastrophic. In contrast, we have shown that athermal systems with a stress overshoot always show brittle yielding at low shear rates, however small the overshoot. It remains to be understood how the thermal scenario crosses over to the athermal one at low temperatures.

The scenarios put forward here differ notably from that recently proposed in mean field [32, 33], in which “duc-

tile” and “brittle” yielding are separated by a critical point, at which the underlying stress-strain curve for homogeneous shear undergoes a qualitative change in shape as the degree of initial sample annealing increases, as sketched in Fig. 1a). To discriminate between the scenario proposed here and that in Ref. [32, 33], it would be interesting to perform particle based simulations that disallow shear banding, to access the shape of the underlying stress-strain curve for homogeneous shear, either by using an algorithm that enforces a homogeneous shear, or simulating a relatively small number of particles, such that no k -mode can become unstable to shear banding. Indeed, Fig. 2D of Ref. [32], reporting simulations for small numbers of particles, gives an indication that the homogeneous stress-strain curve has the form sketched in Fig. 1b,c) above. It further suggests that the smooth athermal yielding seen for modest stress overshoots in [32] may well stem from a finite size effect.

We thank Kirsten Martens, Romain Mari and Matthieu Wyart for discussions; and the SOFI CDT, Durham University, EPSRC (EP/L015536/1) and Schlumberger Cambridge Research for funding.

-
- [1] D. Bonn, M. M. Denn, L. Berthier, T. Divoux, and S. Manneville, *Rev. Mod. Phys.* **89**, 035005 (2017).
 - [2] P. Coussot, *Rheol. Acta* **57**, 1 (2018).
 - [3] D. Bonn and M. M. Denn, *Science* **324**, 1401 (2009).
 - [4] P. Coussot, *Soft Matter* **3**, 528 (2007).
 - [5] M. M. Denn and D. Bonn, *Rheol. Acta* **50**, 307 (2011).
 - [6] T. C. Hufnagel, C. A. Schuh, and M. L. Falk, *Acta Mater.* **109**, 375 (2016).
 - [7] A. L. Greer, Y. Q. Cheng, and E. Ma, *Mater. Sci. Eng. R. Rep.* **74**, 71 (2013).
 - [8] T. Divoux, C. Barentin, and S. Manneville, *Soft Matter* **7**, 9335 (2011).
 - [9] T. Divoux, D. Tamarii, C. Barentin, and S. Manneville, *Phys. Rev. Lett.* **104**, 208301 (2010).
 - [10] T. Divoux, D. Tamarii, C. Barentin, S. Teitel, and S. Manneville, *Soft Matter* **8**, 4151 (2012).
 - [11] V. Grenard, T. Divoux, N. Taberlet, and S. Manneville, *Soft Matter* **10**, 1555 (2014).
 - [12] T. Gibaud, C. Barentin, N. Taberlet, and S. Manneville, *Soft Matter* **5**, 3026 (2009).
 - [13] T. Gibaud, D. Frelat, and S. Manneville, *Soft Matter* **6**, 3482 (2010).
 - [14] T. Gibaud, C. Barentin, and S. Manneville, *Phys. Rev. Lett.* **101**, 258302 (2008).
 - [15] A. Kurokawa, V. Vidal, K. Kurita, T. Divoux, and S. Manneville, *Soft Matter* **11**, 9026 (2015).
 - [16] T. Sentjabrskaja, P. Chaudhuri, M. Hermes, W. C. K. Poon, J. Horbach, S. U. Egelhaaf, and M. Laurati, *Sci. Rep.* **5**, 11884 (2015).
 - [17] C. A. Schuh, T. C. Hufnagel, and U. Ramamurty, *Acta Materialia* **55**, 4067 (2007).
 - [18] P. K. Jaiswal, I. Procaccia, C. Rainone, and M. Singh, *Phys. Rev. Lett.* **116**, 085501 (2016).
 - [19] I. Procaccia, C. Rainone, and M. Singh, *Phys. Rev. E* **96**, 032907 (2017).
 - [20] J. Lin, T. Gueudre, A. Rosso, and M. Wyart, *Phys. Rev. Lett.* **115**, 168001 (2015).
 - [21] C. Liu, E. E. Ferrero, K. Martens, and J.-L. Barrat, *Soft matter* **14**, 8306 (2018).
 - [22] G. P. Shrivastav, P. Chaudhuri, and J. Horbach, *Phys. Rev. E* **94**, 042605 (2016).
 - [23] G. P. Shrivastav, P. Chaudhuri, and J. Horbach, *J. Rheol.* **60**, 835 (2016).
 - [24] A. Wisitsorasak and P. G. Wolynes, *Proceedings of the National Academy of Sciences* **109**, 16068 (2012).
 - [25] G. Parisi, I. Procaccia, C. Rainone, and M. Singh, *Proc. Natl. Acad. Sci. USA* **114**, 5577 (2017).
 - [26] S. K. Nandi, G. Biroli, J.-P. Bouchaud, K. Miyazaki, and D. R. Reichman, *Phys. Rev. Lett.* **113**, 245701 (2014).
 - [27] C. Rainone, P. Urbani, H. Yoshino, and F. Zamponi, *Physical review letters* **114**, 015701 (2015).
 - [28] P. Urbani and F. Zamponi, *Physical review letters* **118**, 038001 (2017).
 - [29] S. Aime, L. Ramos, and L. Cipelletti, *Proc. Natl. Acad. Sci. USA* **115**, 3587 (2018).
 - [30] S. Aime, L. Ramos, J. M. Fromental, G. Prevot, R. Jelinek, and L. Cipelletti, *Rev. Sci. Instrum.* **87**, 123907 (2016).
 - [31] E. D. Knowlton, D. J. Pine, and L. Cipelletti, *Soft Matter* **10**, 6931 (2014).
 - [32] M. Ozawa, L. Berthier, G. Biroli, A. Rosso, and G. Tarjus, *Proceedings of the National Academy of Sciences of the United States of America* **115**, 6656 (2018).
 - [33] M. Popović, T. W. de Geus, and M. Wyart, *Physical Review E* **98**, 040901 (2018).
 - [34] R. L. Moorcroft and S. M. Fielding, *Phys. Rev. Lett.* **110**, 086001 (2013).
 - [35] M. L. Manning, J. S. Langer, and J. M. Carlson, *Phys. Rev. E* **76**, 056106 (2007).
 - [36] M. L. Manning, E. G. Daub, J. S. Langer, and J. M.

- Carlson, *Phys. Rev. E* **79**, 016110 (2009).
- [37] R. L. Moorcroft, M. E. Cates, and S. M. Fielding, *Phys. Rev. Lett.* **106**, 055502 (2011).
- [38] A. Nicolas, E. E. Ferrero, K. Martens, and J.-L. Barrat, *Rev. Mod. Phys.* **90**, 045006 (2018).
- [39] Supplementary material.
- [40] P. Sollich, F. Lequeux, P. Hebraud, and M. Cates, *Phys. Rev. Lett.* **78**, 2020 (1997).
- [41] M. Vasoya, C. H. Rycroft, and E. Bouchbinder, *Physical Review Applied* **6**, 024008 (2016).
- [42] J. Ketkaew, W. Chen, H. Wang, A. Datye, M. Fan, G. Pereira, U. D. Schwarz, Z. Liu, R. Yamada, W. Dmowski, *et al.*, *Nature communications* **9**, 1 (2018).
- [43] M. Singh, M. Ozawa, and L. Berthier, *Physical Review Materials* **4**, 025603 (2020).

Supplemental material: “Ductile and brittle yielding in thermal and athermal amorphous materials”

In this Supplemental Material, we present additional evidence supporting our numerical observations in the main text: that slowly sheared thermal systems show a smooth crossover from “ductile” to “brittle” yielding with increasing height of stress overshoot, and therefore with increasing initial sample annealing prior to shear. In contrast, slowly sheared athermal systems show “brittle” yielding for any height of stress overshoot, however small.

We start in Sec. I by performing a linear stability analysis for the initial onset of shear banding as a system starts to yield, in order to explain our numerical results (separately) for the thermal fluidity and athermal elastoplastic models in the main text. We show that the severity of shear banding (and so of yielding) scales in the limit of slow shear, $\bar{\dot{\gamma}} \rightarrow 0$, as $\exp(\Delta\Sigma)$ in the thermal model, with $\Delta\Sigma$ the magnitude of stress drop from the stress overshoot. Accordingly, in thermal systems a large enough stress overshoot is needed to see severe banding and “brittle” failure. In contrast, in the athermal model the degree of shear strain banding diverges (at the level of our linear calculation) as $1/\partial\gamma\Sigma$ on approach to the stress overshoot, $\partial\gamma\Sigma = 0$. Accordingly, slowly sheared athermal systems are predicted show “brittle” yielding, however small the stress overshoot.

In Sec. II we present additional numerical results supporting those the main text, now in the context of the widely studied soft glassy rheology (SGR) model [40], extended to include explicit spatial stress propagation between elastoplastic elements, and with its noise-temperature parameter, originally intended as a mean field description of this stress propagation, here interpreted as the true thermal energy $k_B T$. In its thermal regime, we show that this gives the same crossover from “ductile” to “brittle” yielding with increasing height of stress overshoot, as for the thermal fluidity model in the main text. In contrast, in its athermal regime it gives the same scenario as the athermal elastoplastic model in the main text, with “brittle” yielding for any size of stress overshoot, however small, in the limit of slow shear, $\bar{\dot{\gamma}} \rightarrow 0$.

Finally in Sec. III, we consider the effects of noise level on when yielding first sets in.

I. LINEAR STABILITY ANALYSIS FOR ONSET OF SHEAR BANDING

A. Thermal fluidity model

To understand the numerical results of Figs. 2 and 3 in the main text for the thermal fluidity model, and to explore the degree to which they might generalise across fluidity models more widely, we cast that model into a

more general form, writing

$$\begin{aligned}\Sigma(t) &= \sigma(y, t) + \eta\dot{\gamma}(y, t), \\ \dot{\sigma}(y, t) &= f(\dot{\gamma}, \sigma, \tau), \\ \dot{\tau}(y, t) &= g(\dot{\gamma}, \sigma, \tau).\end{aligned}\quad (5)$$

The specific fluidity model studied in our numerics in the main text has

$$\begin{aligned}f &= G\dot{\gamma} - \sigma/\tau, \\ g &= 1 - |\dot{\gamma}|\tau/(1 + |\dot{\gamma}|\tau_0).\end{aligned}\quad (6)$$

(plus diffusive terms, which are relatively unimportant in the early stages of any shear banding instability).

To consider the severity with which shear bands will form during any deformation experiment, we write the system's state as the sum of a homogeneous part plus an (initially) small heterogeneous perturbation:

$$\begin{aligned}\dot{\gamma}(y, t) &= \bar{\dot{\gamma}} + \delta\dot{\gamma}(t) \exp(iky), \\ \sigma(y, t) &= \bar{\sigma}(t) + \delta\sigma(t) \exp(iky), \\ \tau(y, t) &= \bar{\tau}(t) + \delta\tau(t) \exp(iky).\end{aligned}\quad (7)$$

The homogeneous part represents an underlying time-dependent base state, as would pertain in a theoretically idealised deformation in which shear bands are not allowed to form. The heterogeneous part is the precursor to any shear bands. Substituting these into the model equations and expanding to first order in the amplitude of the perturbations, we find that the shear rate heterogeneity evolves as

$$d \log(\delta\dot{\gamma})/dt = \omega + d \log(-f_\tau/f_{\dot{\gamma}})/dt. \quad (8)$$

(This expression obtains in the limit of small solvent viscosities $\eta \ll G\tau_0$, small diffusive terms $kl_0 \ll 1$ and slow shear rates $\bar{\dot{\gamma}}\tau_0 \ll 1$, which is the physical regime of interest.) The first term,

$$\omega = -g_{\dot{\gamma}}f_\tau/f_{\dot{\gamma}} + g_\tau, \quad (9)$$

is an eigenvalue which, when positive, indicates an instability to the growth of heterogeneous shear bands. The second term represents a time-dependent spinning of the eigenvector $(\delta\sigma, \delta\dot{\gamma})$. We find numerically that the first term dominates the second after stress overshoot, which is the main regime of interest in these thermal systems. The second term however gives some modest growth of shear banding, even before the overshoot.

For any model of Maxwell-like form, $f = \dot{\gamma} - \sigma/\tau$, and with τ dynamics such that $g_{\dot{\gamma}} = -\tau$, $g_\tau = -\dot{\gamma}$ (which is true for the fluidity model in the main text), it can be easily shown that the eigenvalue

$$\omega = -\partial_t \Sigma. \quad (10)$$

At the level of this linear calculation, therefore, the degree shear banding $\delta\dot{\gamma}(t)/\bar{\dot{\gamma}}$ after any stress drop of magnitude $\Delta\Sigma$ from the stress overshoot scales as

$$\frac{\delta\dot{\gamma}(t)}{\bar{\dot{\gamma}}} = \frac{\delta\dot{\gamma}_0}{\bar{\dot{\gamma}}} \exp(\Delta\Sigma), \quad (11)$$

to within small corrections, where $\delta\dot{\gamma}_0/\bar{\dot{\gamma}}$ is the small background shear rate heterogeneity due to noise. Systems with a small stress overshoot are accordingly predicted to show ductile yielding, and those with a large stress overshoot brittle failure. Because the size of overshoot scales in the fluidity model as an increasing function of $\bar{\dot{\gamma}}t_w$ for low $\bar{\dot{\gamma}}$ (contour lines in Fig. 3 of the main text), deformation experiments with a high $\bar{\dot{\gamma}}t_w$ show brittle failure and those with low $\bar{\dot{\gamma}}t_w$ show ductile yielding for all values of $\bar{\dot{\gamma}}$. This is indeed confirmed numerically in Figs. 2c,d) of the main text.

B. Athermal elastoplastic model

The athermal elastoplastic model studied numerically in the main text considers an ensemble of elastoplastic elements on each streamline. The probability distribution $P(l, y, t)$ of local strains l among these elements on a streamline located at flow gradient position y evolves in time t according to:

$$\dot{P}(l, y, t) + \dot{\gamma}(y, t) \partial_l P = -r(l)P + Y(y, t)\delta(l). \quad (12)$$

The local yielding rate $r(l) = \tau_0^{-1}$ when a local energy barrier E is exceeded, $\frac{1}{2}Gl^2 > E$, and $r(l) = 0$ otherwise, with $G = 1, E = 1$ in our units. Accordingly the threshold yield strain for local yielding $l_c = \sqrt{2}$. The elastoplastic stress on any streamline is the average of the elemental ones: $\sigma(y, t) = G \int dl l P(l, y, t)$. As usual we impose force balance by insisting that the total stress Σ is uniform across streamlines:

$$\Sigma(t) = \sigma(y, t) + \eta\dot{\gamma}(y, t). \quad (13)$$

In the limit of slow shear, $\dot{\gamma} \rightarrow 0$, elements yield essentially instantaneously when they reach the threshold strain l_c . The average elastoplastic stress on any streamline accordingly evolves in this limit according to the simpler equation:

$$\dot{\sigma}(y, t) = \dot{\gamma}(y, t) [1 - l_c P_c(y, t)], \quad (14)$$

in which $P_c(y, t)$ is the probability of an element on a streamline at y having a local strain just below the threshold l_c at time t . (We assume a positive shear rate $\dot{\gamma} > 0$.) Assuming that no element has approached this threshold more than once since shearing started (which is true up to the stress overshoot for most parameter regimes considered), it is trivial to show that $P_c(y, t) = P_0(l_c - \gamma(y, t))$, where $P_0(l)$ is the initial distribution of local strains, giving

$$\dot{\sigma}(y, t) = \dot{\gamma}(y, t) [1 - l_c P_0(l_c - \gamma(y, t))]. \quad (15)$$

To consider the severity with which shear bands will form during any deformation experiment, we write the system's state as the sum of a homogeneous part plus an

(initially) small heterogeneous perturbation:

$$\begin{aligned}\gamma(y, t) &= \bar{\gamma}(t) + \delta\gamma(t) \exp(iky), \\ \dot{\gamma}(y, t) &= \dot{\bar{\gamma}} + \delta\dot{\gamma}(t) \exp(iky), \\ \sigma(y, t) &= \bar{\sigma}(t) + \delta\sigma(t) \exp(iky).\end{aligned}\tag{16}$$

The homogeneous part represents an underlying time-dependent base state, as would pertain in a theoretically idealised deformation in which shear bands are not allowed to form. The heterogeneous part is the precursor to any shear bands. Substituting these into the model equations and expanding to first order in the amplitude of the perturbations, we find in the limit $\eta \rightarrow 0$ that the shear strain heterogeneity after any average imposed deformation to the sample as a whole, $\bar{\gamma}$, obeys:

$$\delta\gamma(\bar{\gamma}) = \frac{\delta\gamma(0)}{\partial_\gamma \Sigma}.\tag{17}$$

It is accordingly predicted to diverge on approach to the stress overshoot, $\partial_\gamma \Sigma = 0$: slowly sheared athermal materials are thus predicted to show “brittle” yielding, however small the stress overshoot.

II. SOFT GLASSY RHEOLOGY (SGR) MODEL

The soft glassy rheology (SGR) model [40] considers an ensemble of elastoplastic elements, each of which corresponds to a local mesoscopic region of material. Given a shear rate $\dot{\gamma}$, each element builds up a local elastic shear strain l according to $\dot{l} = \dot{\gamma}$, giving a shear stress Gl , where G is a constant modulus. This stress is intermittently released by local plastic yielding events, each modelled as hopping of an element over a strain-modulated energy barrier E , governed by a temperature parameter x , with a stochastic yielding rate $r(E, l) = \tau_0^{-1} \min\{1, \exp[-(E - \frac{1}{2}kl^2)/x]\}$, in which τ_0 is a microscopic attempt time [40]. Upon yielding, any element resets its local stress to zero and chooses its new energy barrier from an exponential distribution $\rho(E) = \exp(-E/x_g)/x_g$, which has a characteristic $\langle E \rangle \sim x_g$. This results in a broad spectrum of yielding times, $P(\tau)$, and a glass phase for $x < x_g$, in which a sample shows ageing before deformation commences.

The probability distribution $P(E, l, t)$ of local strains evolves according to:

$$\dot{P}(E, l, t) + \dot{\gamma} \partial_l P = -r(E, l)P + Y(t)\rho(E)\delta(l).\tag{18}$$

Here $Y(t) = \int dl dE r(E, l) P(E, l, t)$ is the ensemble average local yielding rate and $\delta(l)$ is the Dirac delta function. The total elastoplastic stress $\sigma(t) = G \int dl \int dE l P(E, l, t)$.

So far, we have assumed homogeneous flow in the SGR model, without accounting for spatial stress propagation following any local yielding event. To account for non-uniform shear deformations, we now take $n =$

$1 \dots N$ streamlines at discretised flow-gradient positions $y = 0 \dots L_y$, with periodic boundary conditions. The distribution $P(E, l, y, t)$ on any streamline then obeys:

$$\dot{P}(E, l, y, t) + \dot{\gamma}(y, t) \partial_l P = -r(E, l)P + Y(y, t)\rho(E)\delta(l),\tag{19}$$

with streamline yielding rate $Y(y, t) = \int dl \int dE r(E, l) P(E, l, y, t)$ and elastoplastic stress $\sigma(y, t) = G \int dl dE l P(E, l, y, t)$. Given an imposed average shear rate $\dot{\bar{\gamma}}$ across the sample as a whole, the shear rate on each streamline is calculated by enforcing force balance: $\sigma(y, t) + \eta \dot{\gamma}(y, t) = \bar{\sigma}(t) + \eta \dot{\bar{\gamma}}$, with $\bar{\sigma}(t) = \frac{1}{L_y} \int dy \sigma(y, t)$. This ensures 1D stress propagation on a timescale η/G following any local yielding event, recovering the 1D projection of the Eshelby propagator of 2D lattice elastoplastic models [38].

We simulate this model by evolving $M = 80000$ SGR elements on each of $N = 20$ streamlines, with force balance across streamlines as described. Adjacent streamlines are further weakly coupled by adjusting the stress of three randomly chosen elements on each adjacent streamline an amount $wl(-1, +2, -1)$ following any yielding event of size l , with $w = 0.05$ a small parameter. This mimics the stress diffusion term the continuum Eqn. 2 of the main text. We rescale strain, stress, time and length so that $x_g = G = \tau_0 = L_y = 1$. The solvent viscosity $\eta \ll G\tau_0 = 1$ is unimportant to the physics we describe. We use typical values between $\eta = 0.01$ and 0.05 , but find no changes to our results on reducing η further.

It is worth pausing to compare the SGR model studied in this Supplemental Material with the athermal elastoplastic model in the main text. A key difference between the two models is that in the SGR model an elastoplastic element can be activated into yielding even before the top of its energy barrier is reached, by virtue of the temperature parameter, x . In contrast, the elastoplastic model in the main text is athermal. (It sets $x = 0$ upfront.) In some interpretations of the SGR model, x is taken as a mechanical noise temperature. Here we take it to be the true thermal temperature. The other difference between the two models is that the SGR model has a prior distribution of trap depths $\rho(E) \sim \exp(-E/x_g)$, whereas $E = 1$ for all elements in the elastoplastic model in the main text. The combination of the exponential prior with the thermal activation factor captures ageing prior to deformation in the SGR model. In the elastoplastic model of the main text, in contrast, the initial condition at the start of shear must be inserted ‘artificially’ because that model shows no dynamical evolution before deformation commences. The two models are otherwise identical.

We now present numerical results for the predictions of the SGR model for yielding in three different commonly studied annealing protocols. The first protocol is thermal, the second and third are athermal. In each protocol, we seed the formation of shear bands by slightly perturbing the trap depths, after annealing and immediately prior to shear, as $E \rightarrow E [1 + \delta \sin(2\pi y/L_y)]$ with $\delta = 10^{-3}$.

A. Results: thermal SGR model after ageing

We consider first a sample freshly prepared in a rejuvenated state at time $t = -t_w$ then held at a constant temperature in the glass phase $0 < x < x_g = 1$ for a waiting (annealing) time t_w . It is then sheared at a constant rate $\dot{\gamma}$ for all times $t > 0$, with x still held constant. In this protocol, better annealed samples correspond to longer ageing times t_w . It is the same protocol as studied for the thermal fluidity model in the main text, although temperature does not appear as an explicit parameter in that model.

Fig. 6a) shows as dashed lines the underlying stress-strain curves, computed within the SGR model in this thermal protocol, for deformations in which the shear field is constrained to remain homogeneous. Results are shown for several different sample ages t_w at a fixed value of the imposed shear rate. As in Fig. 2a) of the main text for the thermal fluidity model, each curve shows a stress overshoot, the size of which increases with increasing degree of sample annealing before deformation commences (increasing t_w).

The solid lines in Fig. 6a) show the results of separate calculations in which shear bands are allowed to form. For poorly annealed samples, the stress-strain curve closely follows that of the homogeneous calculation, indicating that the deformation remains homogeneous, to good approximation, with no shear bands forming. Yielding accordingly remains a ductile process. For better annealed samples, the stress drops precipitously below that computed when homogeneity is enforced, leading to abrupt yielding. The maximal gradient of stress drop and maximal degree of shear banding in any deformation experiment are plotted as a function of sample age in Fig. 6b). (We define the degree of shear banding as the standard deviation in $\dot{\gamma}$ across y , normalised by the imposed shear rate $\bar{\dot{\gamma}}$.) This shows the same behaviour as for the thermal fluidity model in Fig. 2b) of the main text: the severity of the stress drop and shear banding increase with increasing annealing, t_w , marking a crossover from “ductile” to “brittle” yielding as the height of the stress overshoot increases.

As in the thermal fluidity model, the height of the stress overshoot scales as an increasing function of $\bar{\dot{\gamma}}t_w$. In Fig. 6c) we show results for a fixed large value of $\bar{\dot{\gamma}}t_w$, giving a stress overshoot of fixed large height, for several different values of $\bar{\dot{\gamma}}$. For high $\bar{\dot{\gamma}}$, we see “ductile” yielding, with “brittle” yielding setting in as $\bar{\dot{\gamma}} \rightarrow 0$ (for this fixed large $\bar{\dot{\gamma}}t_w$). In Fig. 6d), we show results for a fixed smaller value of $\bar{\dot{\gamma}}t_w$, giving a smaller stress overshoot. Here we see “ductile” yielding even at very low values of the imposed strain rate. The same scenario was seen in Figs. 2c,d) of the main text for the thermal fluidity model.

To summarise, the SGR model in its thermal regime shows the same scenario as the thermal fluidity model in the main text. This can be seen by the striking similarity between each of the panels of Fig. 6a-d) for the thermal

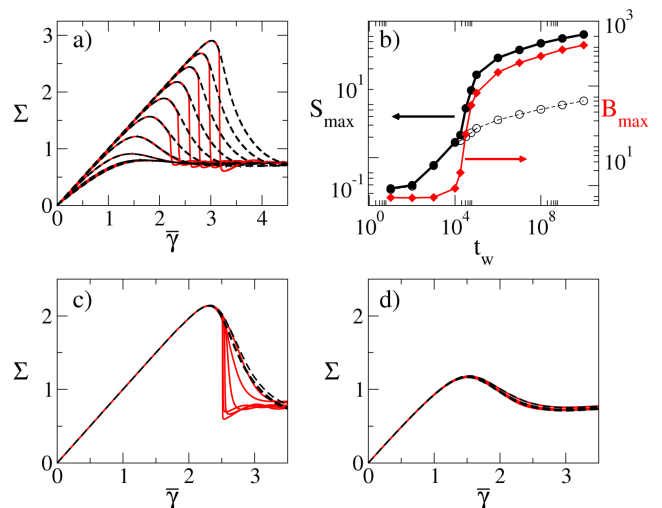


FIG. 6. **a)** Stress versus strain in the SGR model with homogeneous flow enforced (dashed lines) and shear banding allowed (solid lines) for waiting times $t_w = 10^1, 10^2 \dots 10^{10}$ in curves left to right. Imposed shear rate $\bar{\dot{\gamma}} = \sqrt{2} \times 10^{-3}$. **b)** (left vertical axis) steepest negative slope in stress versus strain curve with homogeneous flow enforced (open symbols) and allowing banding (closed black symbols) as function of sample age t_w for a fixed $\bar{\dot{\gamma}} = \sqrt{2} \times 10^{-3}$; (right vertical axis) corresponding maximum degree of shear banding during deformation. B_{\max} and S_{\max} are both averaged over 50 simulations at each t_w . **c)** and **d)** show curves in same format as **a)**, but now for a fixed $\bar{\dot{\gamma}}t_w = 10^4$ giving a large stress overshoot (c) and a fixed $\bar{\dot{\gamma}}t_w = 10$ giving a small stress overshoot (d), for imposed shear rates $\bar{\dot{\gamma}} = 10^{-n}$ with $n = 1.0, 1.5, 2.0, \dots 4.0$ in solid curves right to left in c). Temperature $x = 0.3$.

SGR model with its counterpart in Fig. 2 of the main text for the thermal fluidity model. In particular, in the limit of slow shear, $\bar{\dot{\gamma}} \rightarrow 0$, the severity of shear banding and therefore of yielding increase with increasing height of the stress overshoot, which is in turn set by $\bar{\dot{\gamma}}t_w$.

B. Results: athermal SGR model after slow cooling

We now consider an annealing protocol that consists of equilibrating the sample to a high initial temperature $x = x_0 = 5.0 > x_g$ then cooling to zero temperature at a constant cooling rate α , such that $x(t) = x_0 - \alpha t$, before shearing at a constant rate $\dot{\gamma}$ for all subsequent times, at $x = 0$. In this case, a slower cooling rate α corresponds to a better annealed sample.

Fig. 7a) shows as dashed lines the stress $\Sigma(\bar{\gamma})$ as a function of the accumulating strain $\bar{\gamma} = \dot{\gamma}t$, calculated by imposing that the shear must remain homogeneous across the sample, for several levels of annealing prior to shear, at a single imposed shear rate $\dot{\gamma}$. Each curve shows an initial solid-like elastic regime in which the stress increases linearly with strain, before the stress declines as plastic yielding sets in. As can be seen, more strongly

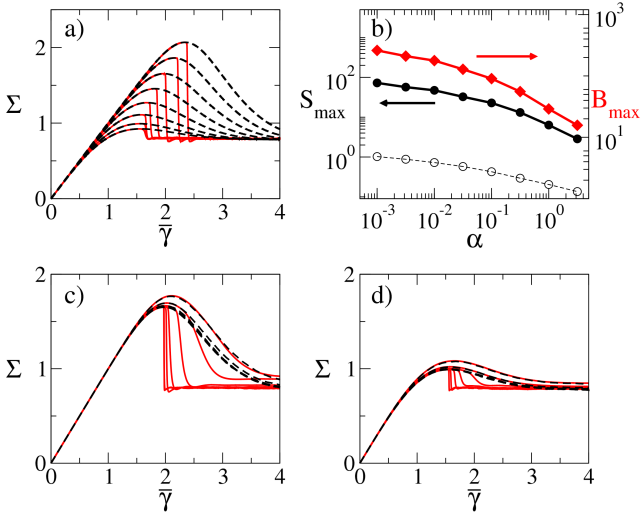


FIG. 7. **a)** Stress versus strain in the SGR model with homogeneous flow enforced (dashed lines) and shear banding allowed (solid lines) for cooling rates $\alpha = 10^{-n}$ with $n = 0.5, 1.0, 1.5 \dots 3.0$ in curves left to right. Imposed shear rate $\bar{\gamma} = \sqrt{2} \times 10^{-3}$. **b)** (left vertical axis) steepest negative slope in stress versus strain curve with homogeneous flow enforced (open symbols) and allowing banding (closed black symbols) as a function of cooling rate α for a fixed $\bar{\gamma} = \sqrt{2} \times 10^{-3}$; (right vertical axis) corresponding maximum degree of shear banding during deformation. B_{\max} and S_{\max} are averaged over 50 simulations at each α . **c)** and **d)** show curves in same format as **a)**, but now for a fixed $\alpha = 10^{-2}$ giving a large stress overshoot (c) and for a fixed $\alpha = 10^0$ giving a small stress overshoot (d), for imposed shear rates $\bar{\gamma} = \sqrt{2} \times 10^{-n}$ with $n = 1.0, 1.5, 2.0, \dots 4.0$ in curves right to left. Temperature $x = 0.0$.

annealed samples (lower α) show a larger initial elastic regime.

We then performed separate calculations in which shear bands can form. The resulting stress-strain curves are shown by solid lines in Fig. 7a). Once the stress overshoot is reached, the stress in these heterogeneous calculations falls precipitously below that of the homogeneous calculations: shear bands form, leading to “brittle” failure. By comparing each of Figs. 7a,c,d) with its counterpart subpanel in Fig. 6a,c,d), we see an important difference between the thermal and athermal regimes of the SGR model. In the thermal regime, a large enough stress overshoot is required to see “brittle” failure. In contrast, in its athermal regime it shows “brittle” failure in slow shear, $\bar{\gamma} \rightarrow 0$, however small the overshoot.

C. Results: athermal SGR model after rapid quenching.

We finally consider an annealing protocol that consists of equilibrating the sample to an initial temperature $x_0 > x_g$, then at some time $t = 0$ suddenly jumping the

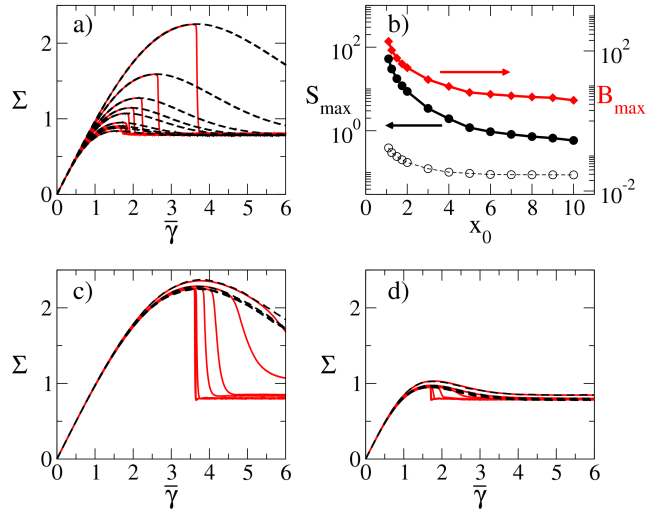


FIG. 8. **a)** Stress versus strain in the SGR model with homogeneous flow enforced (dashed lines) and shear banding allowed (solid lines) for annealing temperatures $x_0 = 1.1, 1.25, 1.5, 1.75, 2.0, 3.0, 4.0, 5.0, 6.0, 7.0, 8.0, 9.0, 10.0$ in curves right to left. Imposed shear rate $\bar{\gamma} = \sqrt{2} \times 10^{-3}$. **b)** (left vertical axis) steepest negative slope in stress versus strain curve with homogeneous flow enforced (open circles) and allowing banding (closed black circles) as a function of annealing temperature, for a fixed $\bar{\gamma} = \sqrt{2} \times 10^{-3}$; (right vertical axis) corresponding maximum degree of shear banding during deformation. B_{\max} and S_{\max} are averaging over 50 simulations at each x_0 . **c)** and **d)** show curves in same format as **a)**, but now for a fixed $x_0 = 1.1$ giving a large stress overshoot (c) and for a fixed $x_0 = 3.0$ giving a small stress overshoot (d), for imposed shear rates $\bar{\gamma} = \sqrt{2} \times 10^{-n}$ with $n = 1.0, 1.5, 2.0, \dots 4.0$ in curves right to left. Temperature $x = 0.0$.

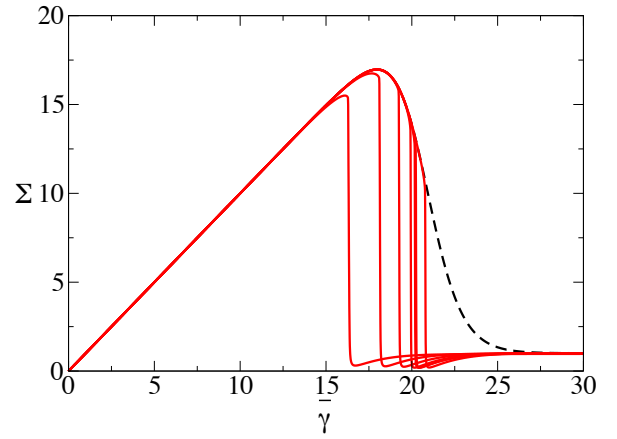


FIG. 9. Stress as a function of strain in the thermal fluidity model of the main text, with homogeneous flow enforced (dashed lines) and shear banding allowed (solid lines), for an imposed shear rate $\bar{\gamma} = 10^{-3}$ and waiting time $t_w = 10^{12}$. Noise levels $\delta = 10^{-n}$ with $n = 3.0, 3.167, 3.33, 3.5, 4.0, 4.5, 5.0$ in curves left to right. Interface width $l = 10^{-3}$. Numerical timestep $Dt = 0.01$, meshsize $Dy = 1/3000$.

temperature to $x = 0$, before shearing at a constant rate $\dot{\gamma}$ for all subsequent times, at $x = 0$. In this protocol, a lower initial equilibration temperature x_0 corresponds to a better annealed sample.

Fig. 8a) shows as dashed lines the stress $\Sigma(\bar{\gamma})$ as a function of the accumulating strain $\bar{\gamma} = \dot{\gamma}t$, calculated by imposing that the shear must remain homogeneous across the sample, for several levels of annealing prior to shear, at a single imposed shear rate $\dot{\gamma}$. Each curve shows an initial solid-like elastic regime in which the stress increases linearly with strain, before the stress declines as plastic yielding sets in. As can be seen, more strongly annealed samples (lower x_0) show a larger initial elastic regime.

We then performed separate calculations in which shear bands can form. The resulting stress-strain curves are shown by solid lines in Fig. 8a). Once the stress overshoot is reached, the stress in these heterogeneous calculations falls precipitously below that of the homogeneous calculations: shear bands form, leading to “brittle” failure. By comparing each of Figs. 8a,c,d) with its counterpart subpanel in Fig. 6, we once again see an important difference between the thermal and athermal regimes of the SGR model. In the thermal regime, a large enough stress overshoot is required to see “brittle” failure. In contrast, in its athermal regime it shows “brittle” failure in the limit of slow shear, $\dot{\gamma} \rightarrow 0$, however small the overshoot.

We have now demonstrated this key difference between yielding in thermal and athermal systems in three ways: (i) numerically by comparing the thermal fluidity model

with the athermal elastoplastic model in the main text, (ii) analytically by performing linear stability analyses in the thermal fluidity model and the athermal elastoplastic model in Sec. 1 of this Supplemental Material and (iii) numerically by comparing the SGR model’s behaviour in its thermal and athermal regimes.

III. EFFECT OF NOISE LEVEL ON YIELDING ONSET

In the main text, we argued that shear banding, and the associated brittle failure to which it leads, arises from a linear instability of a state of initially homogeneous deformation, in the regime where the stress is a declining function of strain. Any linear instability must of course be seeded by noise or initial disorder. We explore finally the effect of noise level on the dynamics of shear banding and yielding. Fig. 9 shows counterpart curves to those of Fig. 2a) of the main text, for the particular value $t_w = 10^{12}$, now for different levels of the noise δ . As can be seen, for increasing δ the stress drop indicative of shear banding occurs earlier and earlier. Indeed, for large enough δ it can occur even before the regime of declining stress versus strain for an underlying state of homogeneous deformation, and therefore before the eigenvalue signifying instability to banding becomes positive in a thermal system. The nucleation of a transition via a finite amplitude perturbation before a regime of linear instability is well known in the context of equilibrium phase transitions. It was discussed with regards yielding of amorphous materials in Ref. [33].